10

Photonic Crystal Fibre for Dispersion Controll

Zoltán Várallyay[1] and Kunimasa Saitoh[2]
[1]*Furukawa Electric Institute of Technology Ltd.*
[2]*Hokkaido University*
[1]*Hungary*
[2]*Japan*

1. Introduction

The idea to prepare photonic crystal fibres (PCF) as their name show, goes back to the birth of photonic crystals. The ability to tailor structures on the micro and nano scale range, in the late 1980s, provided the opportunity to investigate the relation between the structure of matter and light. Three dimensional photonic crystal structures are periodic, dielectric structures in which light may behave similar way as electron waves in a crystal lattice: under suitable circumstances, the periodic potential presented by the crystal may open up a frequency band in which the propagation of electron waves with certain energies are prohibited. This frequency band in the case of photonic crystals is generally called photonic bandgap (PBG) as a nomenclature borrowed from solid state physics. Within this framework, the photonic crystal emerged and became an extensively studied scientific area since 1987 (Yablonovitch, 1987; John, 1987).

To introduce two dimensional photonic crystal waveguides into the practice which implies a waveguide being uniform along the propagation direction holding a two dimensional periodic photonic crystal lattice around the core as shown in Fig. 1, was justified by the novel optical properties of these waveguides compared to traditional optical fibres. One may distinguish two type of photonic crystal PCFs. One type is index guiding PCF (Knight et al., 1996) which means that the core refractive index is larger than the average index of the cladding therefore the propagation occurs due to the total internal reflection on the core-cladding interface and only the fibre structure recalls the structure of photonic crystals. The other type of PCFs is bandgap guiding fibres (Knight, Broeng, Birks & Russell, 1998; Cregan et al., 1999) where the fibre core has lower refractive index than the average index of the surrounding cladding region and the propagation occurs due to the bandgap guidance and not due to the total internal reflection which would not be possible in such a structural arrangement. Both type of PCFs hold very interesting new properties for manipulating and controlling the propagating light or light pulses.

Index guiding photonic crystal fibres with small-core sizes can have a large waveguide contribution to the material dispersion, therefore anomalous dispersion can be achieved well below the 1.27 μm region where material dispersion alone is negative (Mogilevtsev et al., 1998). This allows the dispersion management of the fibres even in the visible wavelength range with a suitable cladding design by changing the hole size and hole-to-

Source: Frontiers in Guided Wave Optics and Optoelectronics, Book edited by: Bishnu Pal,
ISBN 978-953-7619-82-4, pp. 674, February 2010, INTECH, Croatia, downloaded from SCIYO.COM

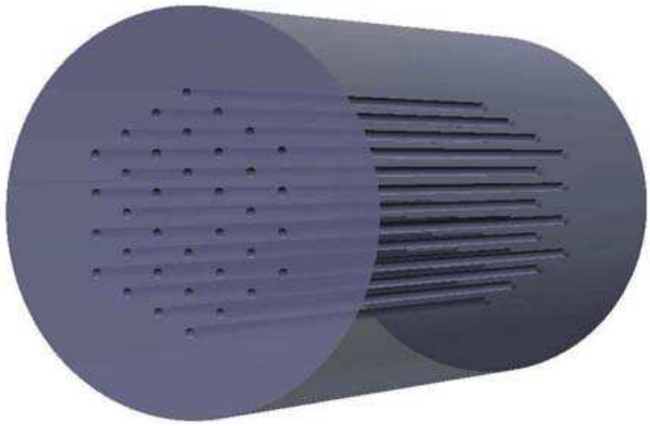

Fig. 1. General scheme of a piece of photonic crystal fibre. Crystal lattice with three periods is illustrated with the missing center most node forming the core. Crystal nodes may consist of holes or low index materials for index guiding fibres and high index glass or liquids for bandgap fibres.

hole spacing (Ferrando et al., 2000; Saitoh et al., 2003). These types of fibres opened up new areas in nonlinear optics such as ultra-broad supercontinuum generation in silica microstructured fibres even in the visible range (Ranka et al., 2000). The process of continuum and super-continuum generation had been known for many years but initial experiments used very high power lasers with large pulse energies (above micro-Joule) and ultra short pulses (< 1 ps), focused into glass, sapphire or even water. The breakthrough provided by photonic crystal fibre in 2000 was the design of the fibre that allowed the use of much lower pulse energies (~1-2 nJ) to produce the continuum effect and the zero dispersion wavelength of the fibre could be close to the pump wavelength of Ti:Sapphire. The continuum is also particularly broad, often spanning over two optical octaves. These novel light sources are cheap and effective sources for spectroscopy, frequency metrology and optical coherent tomography.

Dispersion tailored PCFs also made possible to use these fibres in Ytterbium fibre laser oscillators as a dispersion compensating element because other type of silica glass fibres have normal dispersion at around 1 micron. The obtain pulse widths was approximately 100 fs this way with pulse energy of 1 nJ in an all-fibre arrangement (Lim et al., 2002).

Ultrashort pulse generation via nonlinear compression is also reconsidered at low pulse energies (< 1 nJ) around 800 nm (Várallyay et al., 2007) where the 10 fs region in pulse duration was achieved experimentally by the utilization of dispersion tailored PCF having a zero dispersion wavelength at 860 nm and effective area of 5 μm^2. Theory showed that under optimal conditions the sub-6 fs region can be reached with the same pulse energies and fibre.

Index guiding photonic crystal fibres with sub-micron core diameter was also prepared. These waveguides are usually called nano-wires (Tong et al., 2003). These fibres can provide suitable conditions for ultra broadband soliton-effect compression of femtosecond pulses. In an experiment, 6.8 fs, few-cycle duration was demonstrated starting from 70 fs pulses around 800 nm (Foster et al., 2005) and simulations predicted that self-compression down to single-cycle duration is possible. This compression technique using photonic nanowires provides a simple method for the self-compression of sub-nJ pulses to few-cycle durations without any additional optical elements.

Further useful property of index guiding PCFs that the core size can be scaled well above the core size of single mode step-index fibres without loosing the single-mode operation. Large-mode area photonic crystal fibres yields the possibility of carrying only the fundamental mode in a large mode area decreasing this way the nonlinearity in these fibres for high energy pulse transmission (Knight et al., 1998; Birks et al., 1997; Mortensen et al., 2003). Using ytterbium doped, large mode area PCF higher than 1000 μm^2 effective core area was reported without losing the single mode operation in a fibre amplifier (Limpert et al., 2004). Exceeding the 2000 μm^2 effective core area in a chirped pulse amplifier system was also demonstrated still having the diffraction limited output (Limpert et al., 2006). Doped microstructured fibres are excellent candidates for solely fundamental mode amplification due to the escaping higher order modes between the holes running along the fibre cladding. Bending loss however can be significant and the fibre has to be kept straight. The dispersion of these fibres can not be tailored using structural modifications in the cladding since the waveguide contribution becomes negligible at large core sizes, therefore the dominant dispersion is material dispersion.

Bandgap guiding fibres with a hollow core was first demonstrated in 1998 (Knight et al., 1998). Photonic bandgap fibres enable light guidance in a low refractive index material such as air, vacuum or gas that way that the surrounding cladding is made of a higher index dielectric material such as silica glass. Significantly high percentage of the light energy is guided in the hollow core in the bandgap if surface modes or leaking modes do not affect the propagation. This may offer a significantly reduced nonlinearity with respect to silica core fibres (Lægsgaard et al., 2003; Ouzonov et al., 2003).

Lower loss than in conventional solid core fibres are theoreticaly also achievable (Roberts et al., 2005) as well as light transmission at wavelengths where the material absorption would otherwise be prohibitive (Stephens et al., 2004; Shephard et al., 2005). These properties are uniq features of these waveguides which would not be available without the existance of photonic bandgap effect.

The low nonlinearity and low loss is advantageous for high intensity pulse transmission which is an intended property in laser physics for delivering high power, focused laser beams through fibres. A suitable dispersion profile is however indispensable for ultrashort pulse applications where pulse broadening and pulse distortions may occur very quickly due to improper dispersion management. Photonic bandgap fibres have a typical third order function-like dispersion function (Müller et al., 2002; Jasapara et al., 2003) which increases continuously from the normal dispersion region to the anomalous one with an inflection point in the middle of the bandgap. In order to see this property of bandgap fibres we calculated the dispersion function in a few types of fibres plotted in Fig. 2. This behavior is independent of the constituting materials but it is a basic feature of the bandgap guidance (Bouwmans et al., 2003). The dispersion function of bandgap fibres usually show an anomalous dispersion around the center of the bandgap and it crosses zero close to the short wavelength edge of the bandgap. The monotonically increasing function from the short to long wavelengths shows a significant positive dispersion slope anywhere in the bandgap which limits the compression ratio (Ouzounov et al., 2005) or the quality of the compressible, ultra short pulse (Lægsgaard & Roberts, 2008).

The shape of the dispersion function of photonic bandgap fibres is however affected by the waveguide contribution at small core sizes and by resonances at even large core sizes (Jasapara, Bise, Her & Nicholson, 2003; Jasapara, Her, Bise, Windeler & DiGiovanni, 2003). Harmful effects such as mode anti-crossing (Saitoh et al., 2004; Humbert et al., 2004), surface and leaking modes (Várallyay et al., 2008) may also affect the dispersion function of PCFs.

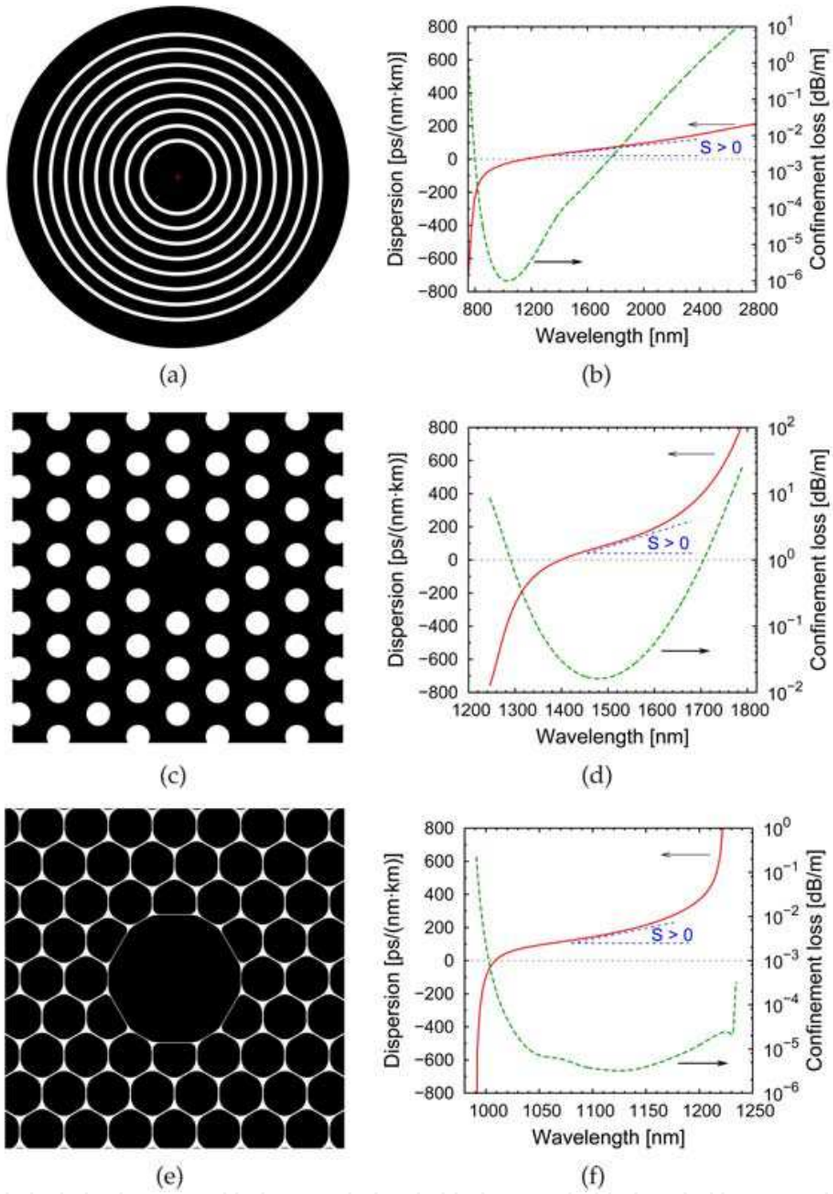

Fig. 2. Structure and dispersion function of different photonic bandgap fibres calculated with the finite element method. *S* refers to the dispersion slope which is clearly positive in all cases. (a) Solid core Bragg fibre with silica (low index regions) and doped silica (high index, white regions). The optimized structure is detailed in Sec. 3.1, (b) obtained dispersion and confinement loss curves with an extra broad bandgap of the annular structure having a full (C_∞) symmetry, (c) silica microstructured fibre where the holes are filled with a high-index liquid. The structure is same as measured in (Jasapara, Bise, Her & Nicholson, 2003): pitch Λ= 5.5 μm, hole diameter d = 2.2 μm and the refractive index of the liquid was n_H = 1.59, (d) obtained dispersion and loss functions for the high index liquid filled PC fibre with a close agreement to the measurements, (e) Structure of a hollow-core fibre with honey-comb cladding and high air-filling fraction. This fibre is used in later calculations and the structure is described in Sec. 4 and (f) the obtained dispersion and loss profiles of the hollow-core fibre.

Namely, an ideal fibre compressor or dispersion compensation unit should posses the following properties to fulfil the requirements in high power, ultra-short pulse compression which is applicable in fibre lasers (Nielsen et al., 2006; Ruehl et al., 2007) as well as in fibre amplifier technology (de Matos et al., 2003):

- low loss
- low nonlinearity (air-guidence or large core size)
- anomalous dispersion (where dispersion is normal otherwise)
- negative or flat dispersion slope in a broad wavelength range.

The last item is believed that it can be realized by structural modifications in photonic bandgap fibres such as introducing resonant layers (Várallyay et al., 2009) which resembles to that of Gires-Tournois interferometers (theory is explained in Sec. 2).

The modification of the dispersion function of bandgap guiding PCFs due to the above mentioned advantageous properties are in high interest. Introducing geometrical defects and resonances in the perfectly periodic structure of a PBG cladding results in a modified groupdelay dispersion and even negative dispersion slope was investigated first in hollow-core OmniGuide fibres (Engeness et al., 2003). Dispersion modification in all-glass PBG fibres was also initiated by the introduction of defect rods in the cladding region (Fang et al., 2007) which theoretically results in resonance behavior. This modification shifted and changed the magnitude of the dispersion function but it preserved the canonical form of the dispersion profile. It was also shown that dispersion modification did work for hollow-core PBG fibres by changing the first period of the fibre suppressing this way the anti-crossing events within the bandgap (Roberts, 2007). The resulted dispersion function is a nearly flat function over a wide wavelength range with very small positive dispersion slope. Negative dispersion slope for hollow-core fibres is also predicted by resonant layers changing the hole size and the shape of the holes in the first and second periods of a hollow-core fibre (Lægsgaard et al., 2007). We showed however that detune the parameters of the first period compared to other periodes of a hollow-core, all-silica Bragg fibre may result in a reversed dispersion slope ($S < 0$ instead of $S > 0$) which can be theoretically considered as an equivalent of a thin-film Gires-Tournois interferometer (Várallyay et al., 2008b; Várallyay et al., 2008). The same was shown for solid core PBG fibres where the freedom of introducing resonant layers is completed by the ability of changing the refractive index of a particular layer (Várallyay et al., 2008a).

In this chapter we present a complete analysis on the possibilities of modifying the dispersion of PBG fibres including solid-core and hollow-core photonic crystal fibres by applying two dimensional, resonant Gires-Tournois interferometers around the fiber core.

2. Theory

We aim to apply resonant structures in PBG fibre claddings resembling to that of Gires-Tournois interferometers (GTI) in solid-core and hollow-core fibres taking the analogy from one dimensional PBG structures. GTIs have an arrangement similar to Fabry-Pérot interferometers. Whereas Fabry-Pérot cavity is enclosed by two high-reflecting mirrors, GTI consists of both a high and a low reflector which results in a highly frequency dependent phase shift on the light field falling on the low-reflectivity surface (Kuhl & Heppner, 1986).

In order to provide a qualitative description of resonances we start with one dimensional photonic bandgap structures which can be associated by dielectric mirrors. The assembly of

alternating high and low index thin films can be characterised by the characteristic matrix of the arrangment having N layers and neglecting the absorbance the following expression can be given (Macleod, 2001)

$$\begin{bmatrix} B \\ C \end{bmatrix} = \left\{ \prod_{q=1}^{N} \begin{bmatrix} \cos(\delta_q) & i\sin(\delta_q)/\eta_q \\ i\eta_q \sin(\delta_q) & \cos(\delta_q) \end{bmatrix} \right\} \begin{bmatrix} 1 \\ \eta_m \end{bmatrix} \tag{1}$$

where

$$\delta_q = k n_q d_q \cos(\theta_q) \tag{2}$$

with $k = 2\pi/\lambda$ the free-space wavenumber, n_q and d_q are the refractive index and physical thickness of the qth layer, respectively and η_q is the addmittance of the same layer at oblique incidence for the p and s-polarization components can be written as

$$\begin{aligned} \eta_q &= n_q Y/\cos(\theta_q) \quad \text{for } p\text{-polarisation (TM)} \\ \eta_q &= n_q Y \cos(\theta_q) \quad \text{for } s\text{-polarisation (TE)} \end{aligned} \tag{3}$$

where $Y = \sqrt{\varepsilon_0/\mu_0}$ is the admittance of the free space. In Eq. (1), η_m is the admittance of the substrate or emergent medium. The amplitude reflection coefficient can be calculated from the characteristic matrix as follows

$$\rho = \frac{\eta_0 - A}{\eta_0 + A} \tag{4}$$

where $A = C/B$ can be obtained from Eq. (1). The phase shift on the reflecting wave is now given as a quotient of the imaginary and real part of Eq. (4)

$$\tan(\varphi) = \frac{\Im\rho}{\Re\rho} = \frac{-2\eta_0 \Im A}{\eta_0^2 - (\Re A)^2 - (\Im A)^2} \tag{5}$$

where $\Im$ and $\Re$ stand for the imaginary and real parts, respectively.

Resonant layers can be introduced in the cladding of a particular bandgap fibre by the modification of one or necessarily more layers.

2.1 One resonant layer

Gires-Tournois (GT) interferometer can be considered as a thin film layer in a simple case with 100% reflection at one side where the high reflectance is ensured by the fibre cladding in a PCF and low reflection at the other side: core and thin-film interface as shown in Fig. 3. The amplitude reflection of this layer is given by Eq. (4) where η_0 is the admittance of the incident medium (core) and A is the admittance of the GT layer which can be obtained from the characteristic matrix (Eq. (1)) yielding

$$A = \frac{\eta_m \cos(\delta) + i\eta_1 \sin(\delta)}{\cos(\delta) + i(\eta_m/\eta_1)\sin(\delta)} \tag{6}$$

where η_m is the admittance of the subsequent layers (the cladding) and δ is the phase factor of the positive going wave and now it is given by $\delta = kn_1 d_{GT} \cos(\theta_1)$ using the notation of Fig. 3. Here, d_{GT} is the GT layer thickness, n_1 is the refractive index of the resonant layer and θ_1 is the angle of refraction.

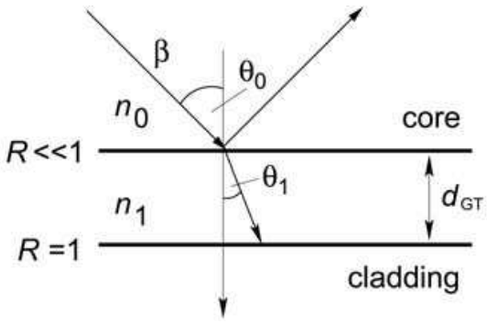

Fig. 3. Schematic illustration of a GT interferometer between core and cladding in a PBG fibre.

η_m can be assumed to be zero in Eq. (6) because the reflectance is 100% = $(\eta_1 - \eta_m)/(\eta_1 + \eta_m)$ at this side of the TF which is a good approximation at the close center of the bandgap.
Writing back Eq. (6) into Eq. (4) with the above mentioned simplification (η_m = 0) the amplitude refraction of a GT interferometer can be given by

$$\rho = \frac{\eta_0 - i\eta_1 \tan(\delta)}{\eta_0 + i\eta_1 \tan(\delta)} \tag{7}$$

The real and imaginary part of Eq. (7) is yielding the phase shift on the incident field as follows

$$\tan(\varphi) = \frac{-2\eta_0\eta_1 \tan(\delta)}{\eta_0^2 + \eta_1^2 \tan^2(\delta)} \tag{8}$$

The group-delay (GD) ($d\varphi/d\omega$), the group-delay dispersion (GDD) ($d^2\varphi/d\omega^2$) and higher order dispersions can be easily derived from Eq. (8). Here, we only give the calculated GD function derived using Eqs. (2) and (8)

$$\frac{d\varphi}{d\omega} = \frac{2\eta_0\eta_1(\eta_0^2 - \eta_1^2)\tan^2(\delta)}{\cos^2(\delta)\left[\eta_0^4 + 6\eta_0^2\eta_1^2\tan^2(\delta) + \eta_1^4\tan^4(\delta)\right]} \frac{d\delta}{d\omega} \tag{9}$$

where $d\delta/d\omega = n_1 d_{GT} \cos(\theta_1)/c$.
The calculation with oblique incidence is essential in the approximation of fiber behavior due to the high propagation angle of light in fibres which prerequisite can be obtained from the corresponding eigenvalue of the investigated mode:

$$\theta_0 = \arcsin(n_{eff}/n_0) \tag{10}$$

where n_{eff} is the effective refractive index and n_0 is associated with the core index.
For the Bragg fibre investigated in Sec. 3.1, the propagation angle obtained from the Helmholtz eigenvalue equation is approximately 87° for the fundamental mode. The

refractive index of GTI is chosen to be n_1 =1.46 which is 0.01 higher than that of the core index which is n_0 = 1.45 at around 1.03 μm. We plot the GD and GDD functions of the GTI based on Eq. (5) in Fig. 4 applying thicknesses that show the nonlinear phase shift and resonance behavior at around 1 μm. We found that the thickness of the GTI must be d_{GT} = 1.34 μm (zeroth-order resonance) or 4.02 μm (first-order resonance). The mediate thicknesses shift the position of the resonance peak as it is indicated by the black solid line in Fig. 4. The reversed dispersion region of the GDD function is broader for the lower-order resonance and sharper for the higher-order one.

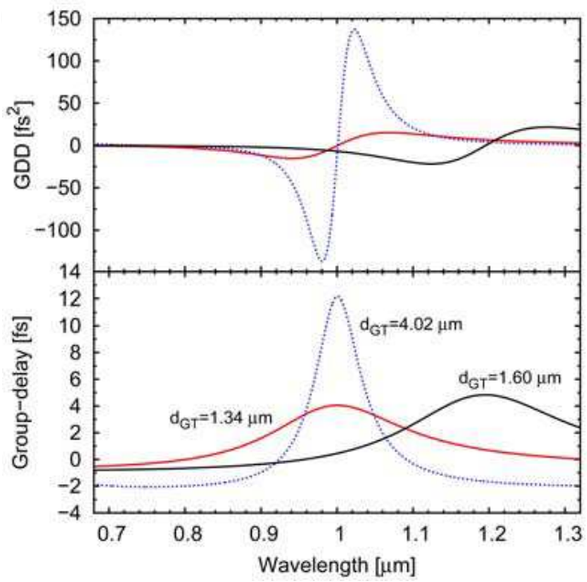

Fig. 4. Zeroth- and first-order resonances on the group-delay and group-delay dispersion curves of Gires-Tournois interferometer for oblique incidence with d_{GT} =4.02 μm and 1.34 μm thicknesses, n_0 = 1.45, n_1 = 1.46 and θ_0 = 87°. Calculated from the derived Eq. (5). Black solid line is a shifted resonance with d_{GT} = 1.6 μm.

2.2 Two resonant layers

There are fibre structures where the introduction of an annular layer around the core having a refractive index close to the core index is not accessible. All-silica hollow core PBG fibres are typical examples where slightly higher index dielectric material than the air is not available, therefore the resonant structure must be set up by changing the thickness of the high index glass and low index air-spacer layers in the same time. Namely the first periode around the fibre core has to be readjusted. This modification as it is shown below must result in the same physical effect as above. A schema of the thin-film model of this arrangement is shown in Fig. 5.

Using the notation of Fig. 5 the characteristic matrix can be written for the two layers in the following form

$$\begin{bmatrix} B \\ C \end{bmatrix} = \begin{bmatrix} \cos(\delta_1) & i\sin(\delta_1)/\eta_1 \\ i\eta_1 \sin(\delta_1) & \cos(\delta_1) \end{bmatrix} \begin{bmatrix} \cos(\delta_2) & i\sin(\delta_2)/\eta_2 \\ i\eta_2 \sin(\delta_2) & \cos(\delta_2) \end{bmatrix} \begin{bmatrix} 1 \\ \eta_m \end{bmatrix} \tag{11}$$

where $\delta_{1,2} = \omega/cn_{1,2}d_{1,2}\cos(\theta_{1,2})$ and $\eta_{1,2} = n_{1,2}Y/\cos(\theta_{1,2})$ for the p-polarization.

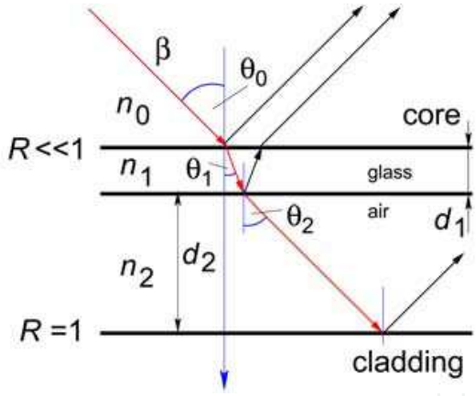

Fig. 5. Schematic of the high and low index layers (first periode) between core and further parts of the cladding having two adjustable thicknesses: d_1 is the physical thickness of the glass layer and d_2 is the thickness of the air-spacer layer.

Performing the operations in Eq. (11) and taking into consideration that $\eta_m = 0$ same as previously, $A = C/B$ is obtained as

$$A = i\frac{\eta_1 \sin(\delta_1)\cos(\delta_2) + \eta_2 \cos(\delta_1)\sin(\delta_2)}{cos(\delta_1)\cos(\delta_2) - \eta_2/\eta_1 \sin(\delta_1)\sin(\delta_2)} \tag{12}$$

Writing back Eq. (12) to Eq. (4) and deriving Eq. (5), one can obtain the phase shift of the incident field upon one reflection given by

$$\tan(\varphi) = \frac{-2\eta_0 \Im A}{\eta_0^2 + A^2} \tag{13}$$

where it was exploited that A has only imaginary part in this particular case.
Assuming a simplified air-silica Bragg structure with annular silica and air layers around the holow core which is analyzed in Sec. 4.1 where we found that the quater-wave stack condition around one micron is fulfiled if the high (silica) and low (air) index layers have the thicknesses of d_H =0.25 μm and d_L =3.9 μm, respectively. The corresponding angle of incidence obtained from Eq. (10) at around 1.05 μm is θ_0 = 86°. We are looking for resonant peaks in the group-delay and reversed GDD function around the 1 μm wavelength region changing the thickness of the first high d_1 and first low d_2 index layers. We plotted three different resonance curves in Fig. 6(a) and 6(b).
Figure 6(a) shows broad resonances with a low index layer thickness $d_2 < d_L$ where d_L is the thickness of the original quater-wave stack for the air layers. Figure 6(b) shows much narrower resonance curves with much sharper peaks having low index thicknesses $d_2 > d_L$. The high index layer was chosen as 0.1, 0.2 and 0.3d_H. One can see that the thiner the glass layer the broader the resonance is. Changing the thickness of the silica layer changes the magnitude of the reflection on the first facet of this combined Gires-Tournois interferometer. Figure 6 is a good illustration for showing that narrower the resonance the steeper the corresponding dispersion curve is.
The phase properties of photonic bandgap fibres can be well approximated with one dimensional dielectric structures (Fekete et al., 2008) using the *p*-polarization component of the light at grazing incidence hence, in the followings, we demonstrate that the calculated GTI works well for solid core as well as for hollow core PBG fibres.

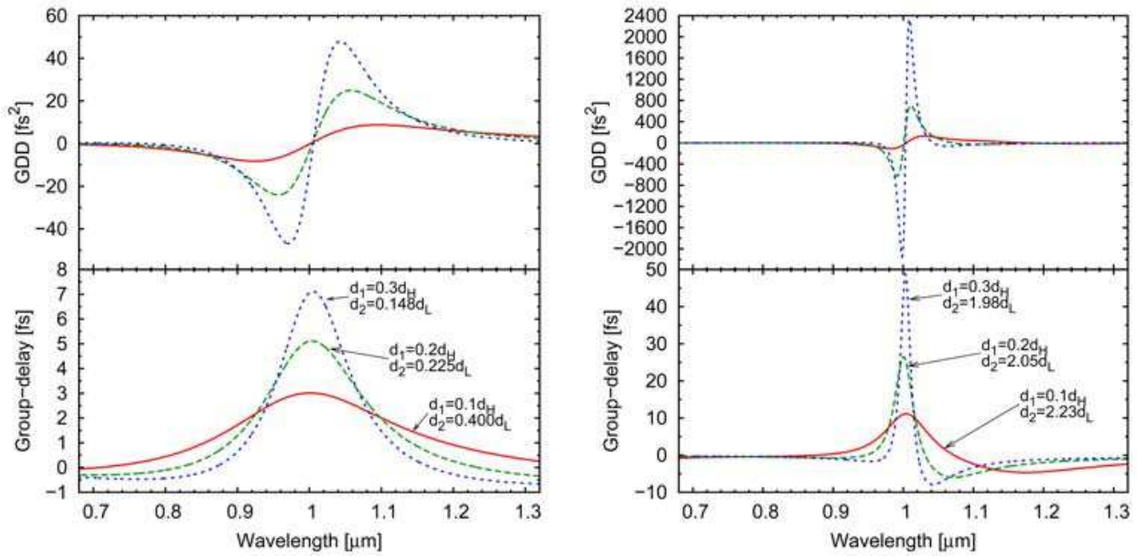

(a) (b)

Fig. 6. (a) zeroth order and (b) first order Gires-Tournois resonances achived by adjusting the first and second high and low index layers assuming a perfectly reflecting underlying cladding ($\eta_m = 0$). The applied thicknesses are expressed in terms of the original quater-wave stacks $d_H = 0.25\ \mu$m and $d_L = 3.9\ \mu$m.

3. Solid core fibres

Bragg fibres analyzed below are not photonic crystal fibres due to the annular arrangement of the alternating high and low index layers not forming a crystal lattice-like pattern . But light guidence is achieved by the bandgap effect similarly to those fibres where a microstructured arrangement ensures the bandgap guidence. Namely the average index of the cladding is higher than the core medium. It is also notable that the first proposition and theoretical analyses on these fibres (Yeh et al., 1978) were presented well before the appearence of photonic crystals and photonic crystal fibres. Bragg fibre can be imagened as a round bent dielectric mirror with properly adjusted high and low index layers for the large angles of incidence of light. In this case the core is an air core and the cladding is formed of the dielectric structure. It is also known however that the loss properties of Bragg fibres are the most advantageous if the core index is identical to the refractive index of the low index layer (Dianov et al., 2009). Therefore the analyses presented below are carried out for such Bragg fibres where the core is a solid, glass core having the same refractive index as the low index layer (same structure was presented in Fig. 2(a)). The introduced resonant layer appeares around the core followed by 8 period of alternating high and low index layers.
We also investigate the properties of solid core photonic crystal fibres with a similar arrangement has shown in Fig. 2(c).

3.1 Solid core Bragg fibre

We realize the same GTI structure in a solid-core Bragg fibre than it is obtained from the analytical calculations in Sec. 2.1. The used structure has shown in Fig. 2(a) and the modified one in Fig. 7. We found that if we use realizable high and low index materials for cladding

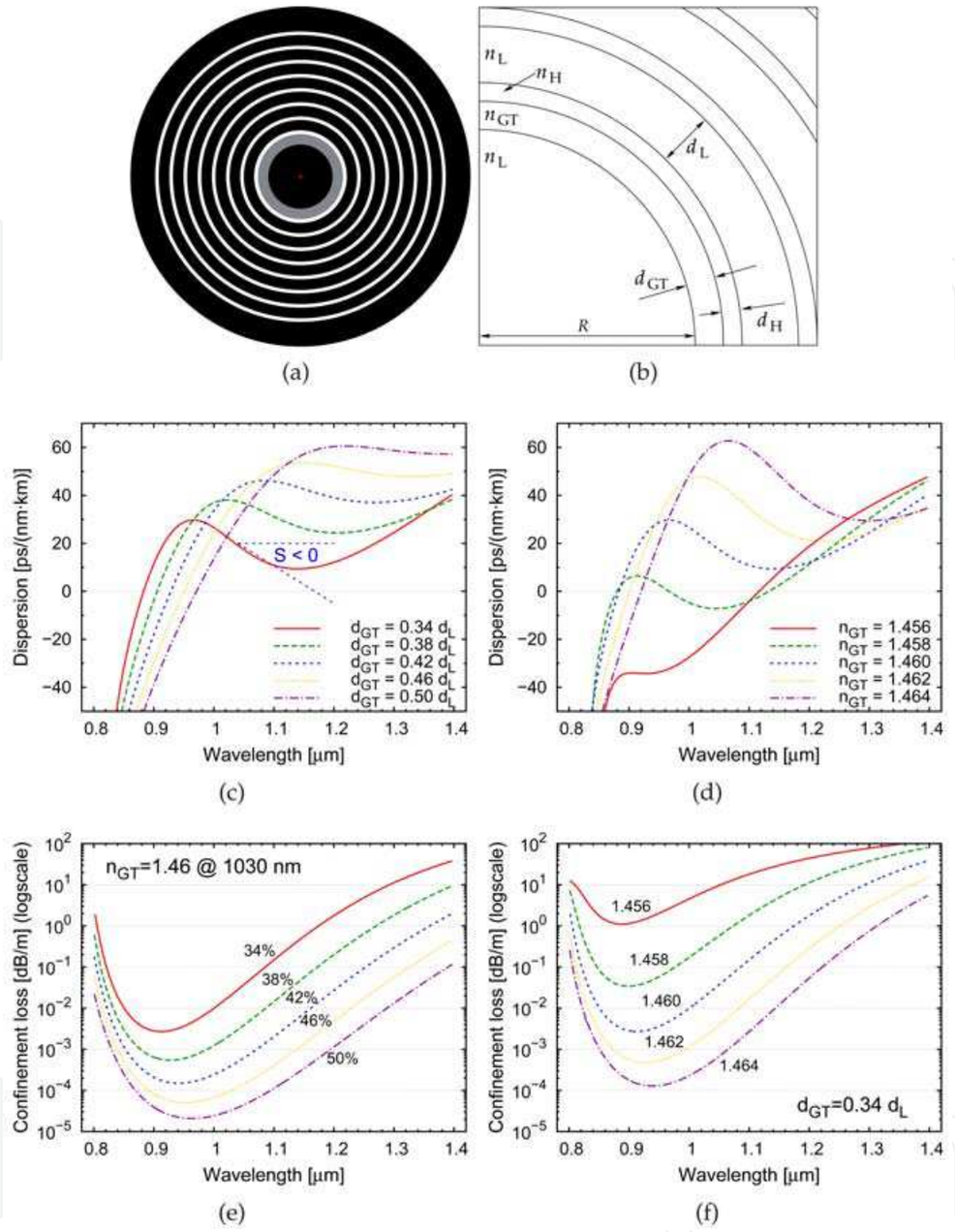

Fig. 7. (a) Solid core Bragg fibre with a resonant first layer just around the core having a refractive index of n_{GT} and thickness of d_{GT}. The original structure is shown in Fig. 2(a), (b) parameters of the fibre: R: core radius, subscripts L and H indicate the low and high index properties, respectively, while GT stands for the resonant GT layer. (c), (d), (e) and (f) shows the obtained dispersion and confinement loss profiles of different GTIs realized around the core in the above Bragg PBG structure. (c) Dispersion functions with different thicknesses of GTI, (d) dispersion functions with GTI having different refractive indices. Dispersion slope (S) is clearly smaller than zero in a broad wavelength range. (e) confinement loss belongs to the case changing GTI thicknesses and (f) confinement loss with different GTI refractive indices.

with n_L =1.45 and n_H =1.5, than the optimum structure which shows a broad and regular bandgap with 10^{-6} dB/m confinement loss must have low index and high index layer thicknesses of 3.8 μm and 0.95 μm, respectively.

Two parameters can be adjusted in connection with the reversed dispersion slope (RDS); the refractive index and the thickness of the GT layer. We set the refractive index of the GT layer to 1.46, and the thickness of it to $0.34d_L$ which results in a 180 nm RDS region from 960 nm to 1140 nm. Increasing the thickness of this resonant layer shifts the RDS region to longer wavelengths (Fig. 7(c)), while the increase in it's refractive index causes stronger resonances and steeper dispersion function due to the decreasing refraction on the first surface (core-GT interface). Figure 7(d) however, shows a high sensitivity on the changes of the GTI index. 0.1- 0.2% index difference may cause almost 100 nm shift and some changes in the steepness of the dispersion slope. This shows that small deviations from the ideal conditions at manufacturing process may result an essentially different dispersion profile.

Nearly zero dispersion profile is also demonstrated in Fig. 7(d) for n_{GT} = 1.458, where the dispersion fluctuation is 12 ps/(nm·km) over a 280 nm wavelength range. Similarly, for d_{GT} = $0.5d_L$ (Fig. 7(c)) the changes of the dispersion function is less than 4 ps/(nm · km) over an almost 200 nm wavelength range. The loss profiles show an acceptable loss (< 0.1 dB/m) for using these fibres in real applications. In Fig. 7(e) and Fig. 7(f), one can see that the wavelength range where dispersion tailoring is achieved falls on the increasing tail of the loss profile which indicates that the mode has continuously stronger resonant coupling with the GT layer, resulting in higher loss. In order to see the changes in the mode profile due to the resonance coupling we plotted the fundamental core mode at the short and long wavelength edge and in the middle of the RDS region in Fig. 8, corresponding to the GTI with $d_{GT} = 0.34d_L$ and $n_{GT} = 1.46$.

The higher the light energy stored in the GTI the larger group-delay of the propagating pulse can be expected as it is already demonstrated at one-dimensional PBG structures (Szipőcs et al., 2000). This is the reason that the introduced resonant layer is able to reverse the dispersion function resulting in a wavelength dependent standing field in the GTI. The mode at the long wavelength edge of the reversed slope looks like more an LP_{02} than an LP_{01} mode due to the resonant coupling of the fundamental mode with the resonant layer (Fig. 8).

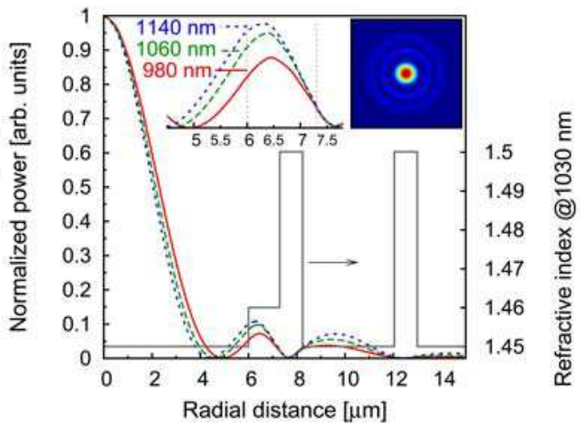

Fig. 8. Propagating fundamental mode profiles at 980 nm, 1060 nm and 1140 nm wavelengths. The embedded graph zooms to the close surrounding of GTI. Vertical black lines show the region where the refractive index n_{GTI} = 1.46. Inset shows the 2D distribution of the propagating fundamental mode at 1060 nm.

3.2 All-glass photonic crystal fibre

All-glass photonic bandgap fibres have pure silica glass core and the cladding consist of cylindrical high-index inclusions forming a crystal lattice. The high-index glass can be dopped silica glass applying germanium oxide. The significance of these fibres lies in the similar property to their index guiding analogons: single mode guidance of the light can be ensured in a broad wavelength range even if the core size is extremaly large (Egorova et al., 2008) and the loss of these fibres are tolarable small for laser applications.

A solid core PCF with photonic bandgap guidence can be an ideal choice to preserve the single modeness at large core sizes keeping low nonlinearity and for the possibility of introducing resonance layers to tailor the dispersion. These fibres are serving many opportunity to introduce the resonant layer in the cladding region, for example, changing the size of the high-index inclusions (d) changing the pitch (Λ), changing the refractive index of the high index glass (n_H) and all the combinations of these changes are available.

In our calculations, we consider an all-silica PCF with a triangular lattice having an index difference between silica and GeO_2 doped silica as large as Δn =0.015. The pitch is Λ=7.4 μm and the hole size is selected to be d =2.47 μm which result in a mode field diameter of ~12 μm around one micron. This structure provide a broad, fundamental bandgap around the 1 μm wavelength range.

The investigated resonant layer is basically that one relates to the theory of GTI with two layers (Sec. 2.2). Namely, the diameter of high index inlaying glass (d_1) and the distance of the first and second periode of the high index regions (Λ_2) are considered as variable parameters. Any other solution such as changing the refractive index of the high index circular inclusions along with varying the geometry is considered in later publications.

Figure 9 shows the dispersion profile and loss profile of the fibre choosing d_1 = 0.741 μm = 0.3d and Λ_2 = 3.11 μm. RDS is achieved between the 1390 nm and 1620 nm wavelengths with an exponentially increasing loss in this range. At the short wavelength edge of the RDS, the confinement loss is 6.8 $\cdot 10^{-3}$ dB/m, at 1550 nm 5 dB/m and at the long wavelength edge, it is almost 100 dB/m. This loss can be decreased by shifting the bandgap to longer

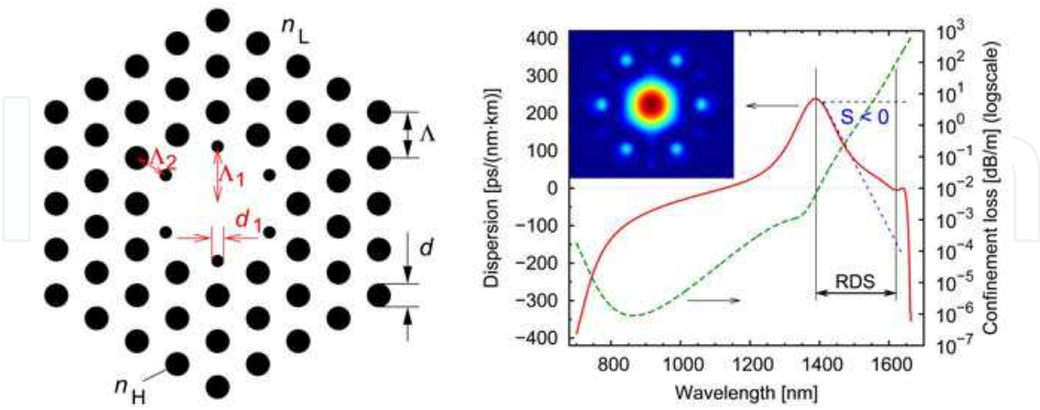

(a) (b)

Fig. 9. (a) Scheme of the structure having a modified first periode in the crystal lattice with smaller diameter of high index region $d_1 < d$ and modified pitch so that $\Lambda_1 > \Lambda_2$ but $\Lambda_1 + \Lambda_2 = 2\Lambda$ (b) Dispersion profile and the corresponding confinement loss curve. RDS is achieved around the telecommunication wavelengths. Inset shows the electric field norm at 1500 nm.

wavelengths by increasing the value of d and Λ and keeping the parameters of the resonant layer for the same value.
The topic to achieve reversed dispersion profile through resonant structures in all-glass photonic crystal fibres is a hot topic in our recent investigations and more detailed analysis on these structures will be presented in later publications.

4. Hollow core fibres

In the followings, we intend to introduce resonant layers in hollow-core, air-silica fibres for the analogy described in the theory in Sec. 2.2. By adjusting the thickness of the first high index layer (core wall) and the following low index layer properly the wavelength dependent nonlinear phase shift on the propagating light may cause a dispersion slope with opposite sign of the conventional bandgap guidence (See Fig. 2(b), 2(d) and 2(f)).
We investigate a simplified, hollow-core Bragg fibre by neglecting the silica struts between the glass annular layers in Sec. 4.1. This type of fibre is intended to combine the advantageous property of Bragg fibres with extra broad bandgaps and the light guidence in a low nonlinearity hollow core region (Vienne et al., 2004).
Due to the significance of small details in PBG structures which are crucial in the design of reliable PBG waveguides, a more accurate model is presented with a honey-comb cladding structure in Sec. 4.2. These type of fibres can be leaking-mode free in a relatively wide wavelength range (Saitoh et al., 2007) therefore the modified dispersion properties can be demonstrated freely. The leaking or surface mode free guidence of light in the case of hollow-core Bragg fibres with support bridges in the low index cladding regions (Foroni et al., 2007) has not been resolved yet. The simplified model however can demonstrate that the theoretical model was presented in Sec. 2.2 is valid for the two-dimensional calculations and explains the underlaying physics.

4.1 Simplified hollow-core Bragg fibre

We use three periods of high (glass) and low (air) index layers in our hollow-core Bragg fibre model (similar to Fig. 2(a) if the dark regions are considered to be the air and white regions the glass). We neglected the effect of silica struts between the glass layers in a first approximation, though these small structural parts modify the effective index of the low index layers by a few percent which requires the modification of the fibre cross-section parameters (Fekete et al., 2008). Silica struts also introduce some mode anti-crossing events partialy due to the lowering of symmetry from full cylindrical (C_∞).
After some optimization of the glass and air layer thicknesses at around one-micron (Várallyay et al., 2008) the critical angle of incidence, the thickness of the low and high index layers were found to be $\theta_0 = 86.16°$, $d_L = 3.92\ \mu$m and $d_H = 0.25\ \mu$m, respectively. The core radius is $R = 10\ \mu$m.
The GTI layer is formed by readjusting the first high and low index layers (first periode) around the core. The thin glass layer plays the role of a partial reflector, and behind the resized low index layer (cavity) cladding acts as a high reflectivity mirror of the two-dimensional Gires-Tournois interferometer. In our present simulation, we choose three different silica (high index) layer thicknesses for partial reflector layers around the core, which are 10, 20 and 30% of the thickness of the high index layers forming the quarter-wave stack Bragg mirror design. The obtained results of the computations in Fig. 10(a) clearly

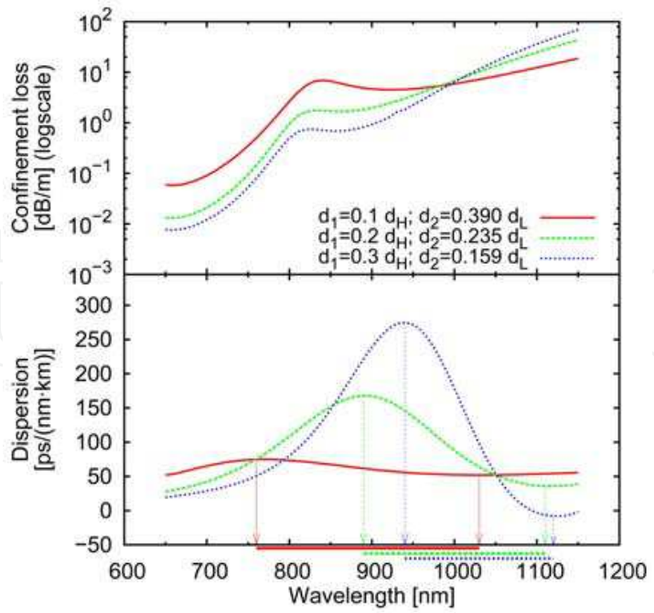

(a)

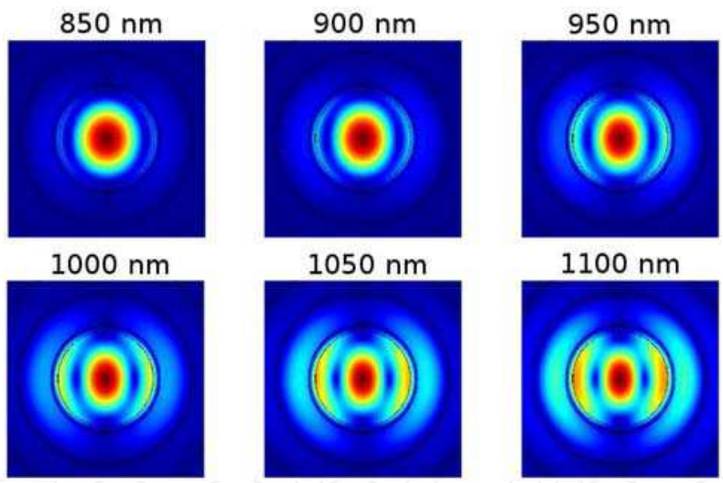

(b)

Fig. 10. (a) Dispersion and confinement loss of the fundamental core mode propagating in hollow-core Bragg fibre corresponding to three different GTI arrangement. Physical thicknesses of the high index partial reflector layers (d_1) and the low index air spacer layers (d_2) forming the resonant layer are expressed in terms of the high and low index quarter-wave stacks. (b) Fundamental mode field distribution with resonant coupling with the GTI in a hollow-core Bragg fibre having a readjusted first periode and design parameters $d_1 = 0.3d_H$ and $d_2 = 0.159d_L$ (blue curve in Fig. 10(a)).

show that RDS can be obtained in a relatively wide wavelength range. In our models, the d_2 spacing between the cladding and the thin partial reflector layer had to be set to 0.39, 0.235 and 0.159 times the spacing between the fused silica layers in the quarter-wave stack design (d_H). The RDS regims corresponding to the different partial reflector layers are 260, 220 and 180 nm, respectively.

The used parameters in the theory (Sec. 2.2) predicted the RDS around one micron accurately compared to the two-dimensional model presented here. Layer thicknesses for GTI are almost exactly the same values predicted analytically and obtained numerically.
In order to have an insight into the physical effect of the cylindrical GTI layer, what we can regard as a realigned first period we computed the mode field distributions at different wavelengths which results are shown in Fig. 10(b). The superimposed GTI layer contribute to the effective index of the LP_{01} mode in a resonant way through the frequency dependent mode field distribution. The ratio between the peak of the transversal mode distribution and side peaks vary around the resonance wavelength similar way was shown in Fig. 8, leads to the desired RDS.

4.2 Hollow core fibre with honey-comb structured cladding

In the case of all-silica hollow-core PBG fibres the resonant GT layer can be presented by the same way was discussed in the previous subsection changing the thickness of the first air layer whose reflectance can be further reduced by decreasing the thickness of the core wall (first high index layer). The high reflector is the properly designed microstructured cladding where the high and low index layers satisfy the quarter wavelength condition. The used model of hollow-core PBG fibre with a honey-comb structured cladding and the necessary geometrical changes are shown in Fig. 11(a) and the corresponding parameters are represented in Fig. 11(b). In a 7-unit-cell hollow-core-PBG fibre, core radius is determined by the hole-to-hole spacing Λ, the core wall thickness t and the introduced core expansion coefficient E

$$R_c = (E+1)(1.5\Lambda - t/2) \tag{14}$$

where the role of E is clearly to provide a larger core and a detuned first period with thin air-spacer layer (parameters are in Fig. 11(b)). The pitch was selected to Λ = 2.85 μm to obtain a bandgap centered around 1100 nm wavelength range and the hole size and pitch ratio to d/Λ = 0.98 which indicates a very high air-filling fraction in order to obtain large PBG in the cladding and lower the leakage losses (Saitoh & Koshiba, 2003). The core wall thickness was $t = T(\Lambda - d)$ where T is a parameter usually smaller than unity. We can suppress the existence of surface modes which localize energy at the core wall by selecting T <0.5 (Saitoh et al., 2007) at the RDS wavelengths.

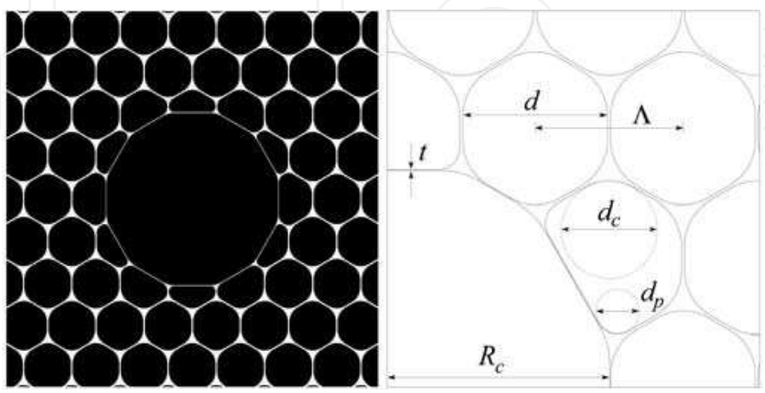

(a) (b)

Fig. 11. (a) the modified fibre structure with an applied core expansion based on the structure was shown in Fig. 2(c) and (b) the model parameters.

In Fig. 12(a), and 12(b) we show the calculated dispersion profiles for the LP_{01}-like fundamental air-core mode for changing the T and E parameters, respectively, in a 7-cell-core PBG fibre. If T = 0.3 and E = 0.18, the obtained dispersion function is the one having a RDS around 1050 nm and it ranges from 1012 nm to 1106 nm. This 94 nm wide reversed slope region presented for the LP_{01}-like fundamental mode can be raised to 120 nm by setting T =0.45 (see Fig. 12(a)). This increase in the core wall thickness introduces stronger resonance in the phase-delay of the light due to the increasing reflectance of the first facet light reaches during the propagation and consequently results in a steeper dispersion slope than those belonging to smaller T values. Decreasing the magnitude of the expansion coefficient (Fig. 12(b)) will shift the reversed slope region to longer wavelengths without changing the magnitude of the negative slope range. Namely, varying the thickness of the first low index layer will determine the position of the resonance property.

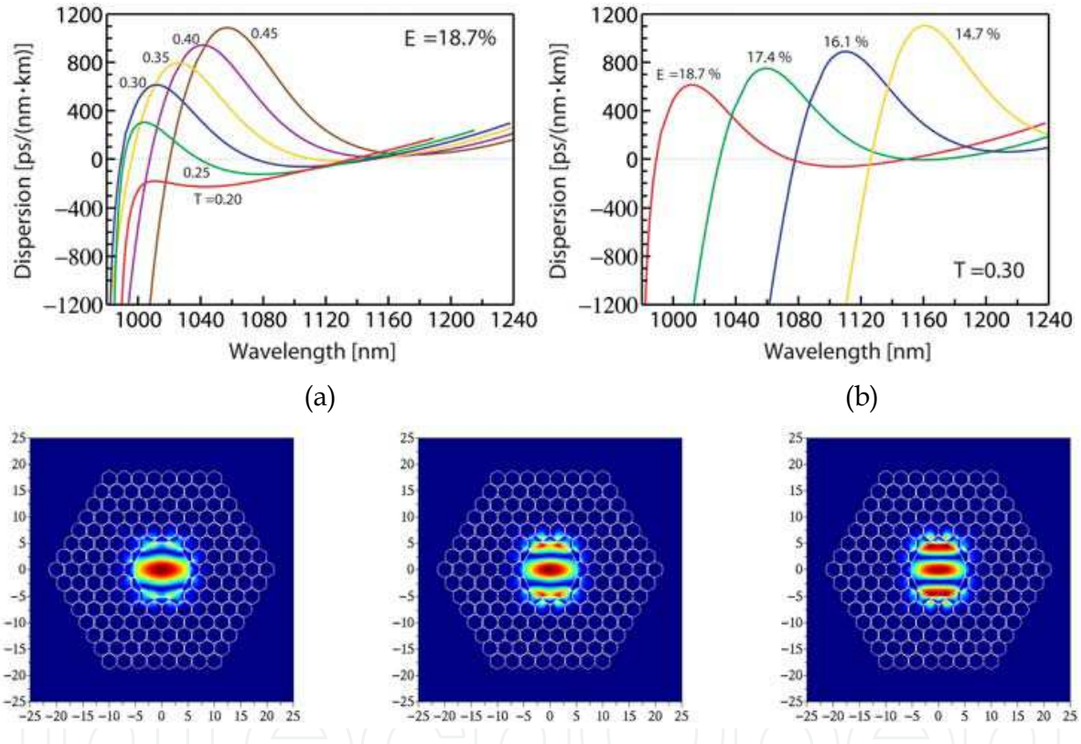

Fig. 12. Dispersion functions of the designed hollow-core PBG fibre with (a) different core wall thicknesses and (b) different core expansion coefficients. (c) Mode distribution for one particular polarization component of LP_{01} at 1000 nm, 1050 nm and 1100 nm.

Because of the large index difference between the low and high index materials constituting the fibre cladding the resonant coupling with the GTI is also larger than in the case of solidcore fibres with smaller index differences, resulting in a much more distorted mode profile. Figure 12(c) shows the mode field distribution at 1000, 1050 and 1100 nm.

Figure 13 is intended to show the wavelength-dependence of the confinement loss for the fundamental air-core mode with and without GTI in hollow-core PBG fibres using 6 periods of air-holes in the cladding region. T is kept at 0.3 in both cases without core expansion as well as with E = 0.187. Due to the presence of resonances for E = 0.187, what we obtained is

an elevated loss profile by almost three magnitudes, but still resulting in less than 0.01 dB/m which is acceptable for the purpose of dispersion management.

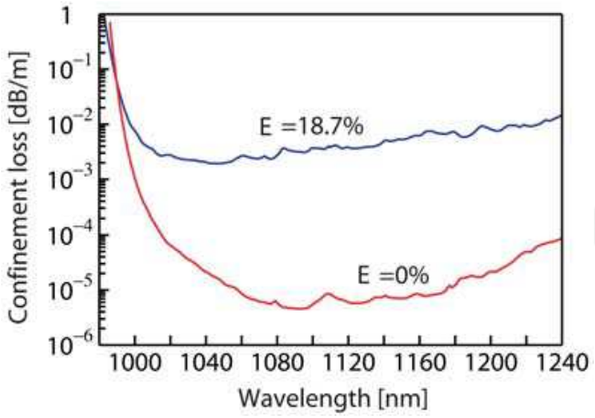

Fig. 13. Confinement losses of hollow-core PBG fibres with $E = 0$ and $E = 0.187$ core expansion factors.

5. Fibre properties

5.1 Coupling loss

Due to the mode distortions it is reasonable to investigate how large coupling loss can be expected when one splices the investigated fibre in Sec. 3.1 to an other Bragg or a step-index profiled fibre. We computed the overlap integral between the modes of the modified cladding structure and the modes of the fibre without GTI:

$$\mu(\lambda) = \int_0^{2\pi} \int_0^{\infty} \Psi^{(1)}(r,\varphi,\lambda)\Psi^{(2)*}(r,\varphi,\lambda) r dr d\varphi \tag{15}$$

where $\Psi^{(k)}$, $k = 1,2$ is the normalized electric field distribution in the kth fibre, and the symbol asterisk stands for complex conjugate. r and φ are the variables of polar coordinates in Eq. (15). The results are summarized in Fig. 14(a) where we present the loss due to coupling the light from one fibre to another one between 900 and 1200 nm. First we tested the coupling between the unmodified Bragg fibre ($d_L = 3.8$ μm, $d_H = 0.95$ μm $n_L = 1.45$ and $n_H = 1.5$) and a step-index fibre having the same 6 μm core radius and an index difference between the core and cladding: $\Delta n = 0.0036$. The cladding refractive index follows the index of fused silica obtained from the Sellmeier equation at any wavelength. The overlap factor shows 81% coupling at 1040 nm which is equivalent with a 0.9dB loss (curve with full circles in Fig. 14(a)). By the introduction of the GT layer around the core in the Bragg fibre ($d_{GT} = 0.34 d_L$, $n_{GT} = 1.46$ at 1030 nm) and investigate the coupling to a Bragg fibre with the same cladding structure except the GTI, the overlap factor yields a value of 30%which corresponds to 5.2dB loss (full squares in Fig. 14(a)). This large coupling loss becomes even larger if we couple the distorted mode field into the step-index fibre (open circles in Fig. 14(a)) where the loss is more than 7.2 dB at 1050 nm.

Fortunately, this large loss can be optimized. If we take a look at the effective indices of Bragg fibres with and without GTI we can see that the difference can be considered

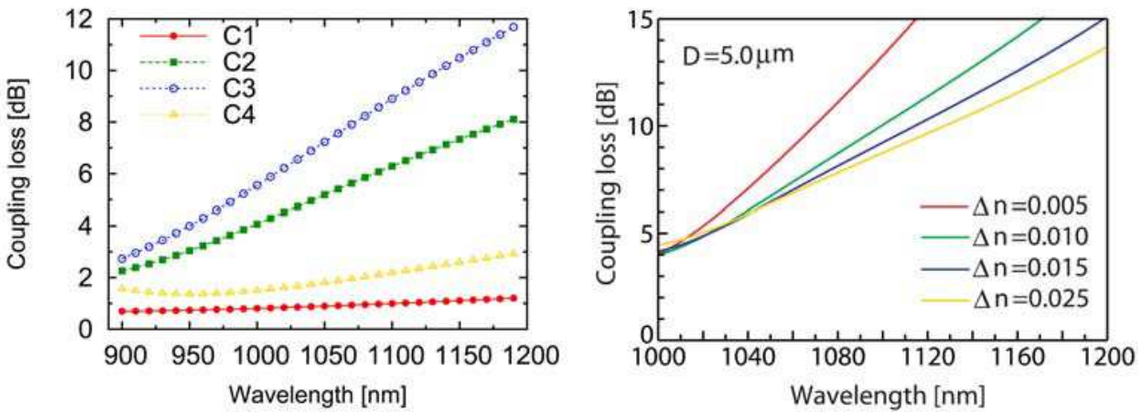

(a) (b)

Fig. 14. (a) Coupling loss calculated from the overlap integral between LP_{01} modes of different fibres. "C1" refers to the coupling between the Bragg fibre without GTI and a stepindex fibre; "C2" is the coupling between two Bragg fibres with and without GTI and both R_c is 6 μm; "C3" is the coupling between step-index and Bragg fibre with GTI and "C4" is the improved coupling between two Bragg fibres with and without GTI by changing the core size of the Bragg fibre without GTI. (b) Coupling loss as a function of wavelength between hollow-core RDS and step index fibres with different index profiles using a core diameter of 5 μm.

significant and should be moved closer in order to obtain a better coupling efficiency. The effective refractive indices are 1.447329 and 1.448562 at 1040 nm for a Bragg fibre with and without GTI, respectively. If we start to decrease the core size of the regular Bragg fibre without GTI, we can decrease the effective index as well, since the wave vector of the propagating mode will enclose a smaller incident angle (see Eq. (10)). For a 4.1 μm core radius of the normal Bragg fibre the effective index is 1.447351 for LP_{01} at 1040 nm and this way the coupling loss becomes less than 1.7dB with the distorted mode (open triangles in Fig. 14(a)).

In the case of hollow-core PBG fibre attaching simply the modified and unmodified structures will result in 4-7 dB loss along the RDS region. Using step-index fibres the loss between the hollow-core RDS and these fibres are even larger. Fig. 14(b) shows the coupling loss between the step-index fibre with different index profiles and the hollow-core RDS fibre where the expansion factor is set to E = 18.7%. The calculations presented in Fig. 14(b) was performed with a step-index fibre having a core size of 5 μm. The coupling loss is found to be between 4 and 9 dB over the RDS range.

We can see also in Fig. 14(b) that the coupling loss can be decreased by increasing the index difference of step-index fibre. Larger mode field diameter is presented for longer wavelengths in index guiding fibres but this larger mode field diameter can be decreased using a fibre with larger index difference. This larger Δn however gains the possibility of multimode operation. The calculated fibre structures are multi-moded which indicate that coupling may occur to higher order modes of the RDS fibre and may degrade the beam quality of the output if it is used for a pulse compressor. Analyses and solutions on this issue require further investigations of these fibres.

5.2 Propagation loss

The propagation loss in optical fibres can be evaluated as a sum of different type of losses such as confinement loss and scattering loss. In the case of using the fibre in a wavelength range where the bandgap is surface-mode and leaking-mode free the dominant loss will be the scattering loss (Roberts et al., 2005).

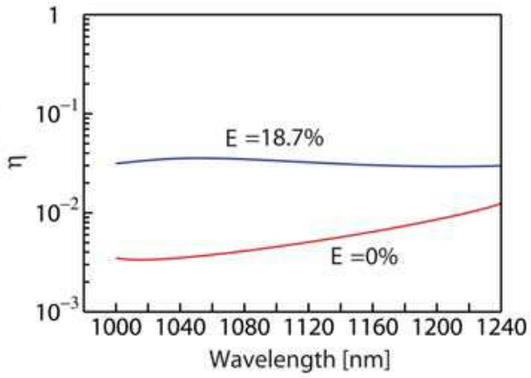

Fig. 15. The η-factor of the fundamental air-core mode as a function of wavelength with $d/\Lambda = 0.98$, $dc/\Lambda = 0.70$, $d_p/\Lambda = 0.30$, $\Lambda = 2.85$ μm, $T = t/(\Lambda - d) = 0.30$, and the expansion coefficient is set to E=0% and 18.7%.

Figure 15 shows the η-factor (Murao et al., 2008) of the fundamental air-core mode in hollow-core fibre as a function of wavelength with $d/\Lambda = 0.98$, $d_c/\Lambda = 0.70$, $d_p/\Lambda = 0.30$, $\Lambda = 2.85$ μm, $t = 0.3(\Lambda - d)$, and the expansion coefficient is set to E=0% and 18.7% (see parameters in Fig. 11(b)), where the η-factor is defined as the normalized overlap integration of the power in the silica-ring as follows:

$$\eta = \frac{\int_{\text{glass annulus}} (\mathbf{E} \times \mathbf{H}^*) \cdot \hat{\mathbf{z}} dA}{\int_{\text{cross-section}} (\mathbf{E} \times \mathbf{H}^*) \cdot \hat{\mathbf{z}} dA} \tag{16}$$

The η-factor, which is proportional to the scattering loss of hollow-core PBG fibres due to the surface roughness of the silica-ring around the air-core. In the hollow-core PBG fibre with GTI, it is about one order of magnitude larger than the scattering loss in the hollow-core PBG fibre without GTI.

5.3 Fibre nonlinearity

The fibre nonlinearity of hollow-core PBG fibres can be almost one thousand times smaller than that of single mode fibres ($\gamma \approx 10^{-6}$ $(\text{Wm})^{-1}$). This value was reported theoretically (Lægsgaard et al., 2003) as well as experimentally (Hensley et al., 2007). The utilization of resonant structures however may increase this value due to the increased guided mode overlap with silica.

In Fig. 5.3, we show the nonlinear coefficient γ as a function of wavelength which is a crucial quantity in high power light delivery. We use the following definition of the nonlinear coefficient (Vincetti et al., 2006)

$$\gamma = \gamma_{\text{air}} + \gamma_{\text{silica}} = \frac{2\pi n_{2_{\text{air}}}}{\lambda A_{\text{eff}_{\text{air}}}} + \frac{2\pi n_{2_{\text{silica}}}}{\lambda A_{\text{eff}_{\text{silica}}}} \tag{17}$$

where n_2 is the nonlinear refractive index coefficient and A_{eff} is the effective mode area calculated for air and silica, respectively, defined as (Lægsgaard et al., 2003)

$$A_{\text{eff}_i} = \frac{\left(\int_{\text{cross-section}} (\mathbf{E} \times \mathbf{H}^*) \cdot \hat{\mathbf{z}} dA\right)^2}{n_i^2 \varepsilon_0^2 c^2 \int_{A_i} |\mathbf{E}|^4 dA} \tag{18}$$

where i = air or silica, ε_0 is the permittivity and c is the speed of the light in vacuum. It can be seen clearly from the results in Fig. 16 that γ is increased for the PBG fibre with GTI with an order of magnitude. The increased nonlinearity may still ensure the validity of using these fibres for high power pulse compression but the available power level with fibres using this type of resonant structure is clearly lower than using low nonlinearity hollow-core fibres. The improvement of nonlinearity is essential in these fibres to introduce them in high intensity pulse compression though we present some solutions which still allow the generation of ultra-short and high energy pulses (Sec. 6).

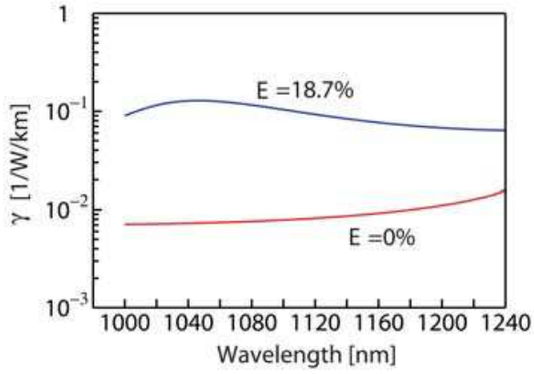

Fig. 16. The nonlinear coefficient γ as a function of wavelength in a 7-cell hollow-core PBG fibre with and without core expansion.

In the case of solid-core fibres we have to account for only the second term of Eq. (17) since we can assume that the nonlinear refractive index of the different glasses are nearly the same. From the calculated $A_{\text{eff}}(\lambda)$ which increases with the increase of the wavelength, solid-core fibre nonlinearity shows an opposite behavior than hollow-core fibre (Várallyay et al., 2009). This is due to the expansion and larger penetration of the mode into the cladding region as a function of wavelength. This phenomenon is the same in the two types of fibres but the larger fraction of pulse power in the cladding of hollow-core fibres results in the significantly larger silica contribution to γ increasing it's value.
We obtained that the nonlinear coefficient of hollow-core RDS fibre is still more than a magnitude smaller than in solid-core PBG fibres at around 1050 nm (Várallyay et al., 2009). The increase of core size may lower the nonlinearity in solid-core fibres but this changes limit the wavelength range of the resonance since the propagation angle of the mode gets closer to the right angle.

6. Propagation analysis

We investigate a pulse compressor consisting of two serially connected hollow-core fibres with and without RDS. In the case of linear propagation, the necessary fibre lengths for

compensating the chirp on a broadband pulse up to the third order can be estimated from the following equation-system

$$\beta_2^{(1)} L^{(1)} + \beta_2^{(2)} L^{(2)} + GDD_0 = 0 \tag{19}$$

$$\beta_3^{(1)} L^{(1)} + \beta_3^{(2)} L^{(2)} + TOD_0 = 0 \tag{20}$$

where $\beta_i^{(j)}$ is the ith order term in the Taylor series of the dispersion of the jth fibre, $L^{(j)}$ is the length of the jth fibre and GDD_0 and TOD_0 are the pulse initial GDD and third-order dispersion (TOD), respectively. It can be seen from Eq. (19) and (20) if the input chirps of the pulses are zero the pulse shape will be preserved when the ratio of the third and second order dispersion terms are same for the two fibres.

Self-phase modulation adds some additional chirp on the pulse in the case of nonlinear propagation which depends on the actual pulse power. The propagation is treated by the generalized nonlinear Schrödinger equation (Agrawal, 2007)

$$\frac{\partial E(z,t)}{\partial z} + \left(\sum_{k=2}^{N} \beta_k \frac{i^{k-1}}{k!} \frac{\partial^k}{\partial t^k} \right) E + \frac{\alpha}{2} E = i\gamma \left(|E|^2 E + \frac{i}{\omega_0} \frac{\partial}{\partial t} \left(|E|^2 E \right) - T_R E \frac{\partial |E|^2}{\partial t} \right) \tag{21}$$

where E is the complex envelope function, z is the coordinate in the propagation direction, t is the retarded time, α is the attenuation coefficient, β_k is the kth order dispersion from the Taylor-series of the propagation constant, γ is the nonlinear coefficient and T_R is the first moment of the nonlinear Raman response. Eq. (21) is solved by the split-step Fourier method (Agrawal, 2007) such a way that the maximal phase change of the propagating pulse remained below 0.01 radian.

The GDD and 3rd order dispersion values of the regular and RDS fibres are −0.07748 ps^2/m, 0.00036 ps^3/m and −0.05847 ps^2/m, −0.00309 ps^3/m, respectively. The nonlinear coefficient (γ) of the two fibres are $7 \cdot 10^{-6}$ and 10^{-4} 1/(Wm) based on the calculations presented in Sec. 5.3. Detailed simulation parameters including higher order dispersion values, pulse and additional fiber parameters are same as used in (Várallyay et al., 2009).

The first guess for the lengths of the fibres is taken from Eq. (19) and (20) and a brute-force optimization is used to find the highest peak power around the initial guess which target yields the possible shortest pulses with the possible highest quality (Várallyay et al., 2007).

We calculate the propagation and compression of Gaussian pulses with $5 \cdot 10^5$ fs^2 linear input chirp and over 16 nm bandwidth. The resulted input pulse width is 11.1 ps. This magnitude of input chirp can be a realistic value for pulses coming out from fibre oscillators or amplifiers. The dispersion parameters up to the fifth order is taken into consideration for both type of hollow-core fibres (see (Várallyay et al., 2009)). Dispersion properties of hollow-core RDS is fitted to the dispersion function obtained from the calculations which belong to the parameters E = 0.187 and T = 0.3 (see Fig. 12). The dispersion function of the regular hollow-core PBG fibre is fitted to a HC-1060 type fibre (see, for instance, in Ref. (Saitoh et al., 2003)). The β_3 parameter has a different sign in the two fibres and an approximately ten times larger absolute value for hollow-core RDS fibre than HC-1060. The coupling loss between the two fibres is assumed to be 5 dB.

The calculations are shown in Fig. 17(a) and 17(b). In this case the combined fibre compressor yields 1.5 times shorter pulses with significantly better pulse quality (QF=90.6%)

compared to the performance of regular hollow-core fibres. The HC-1060 type fibre can compress the 100 nJ pulses with 74.3% QF after 6.3 m length of propagation.

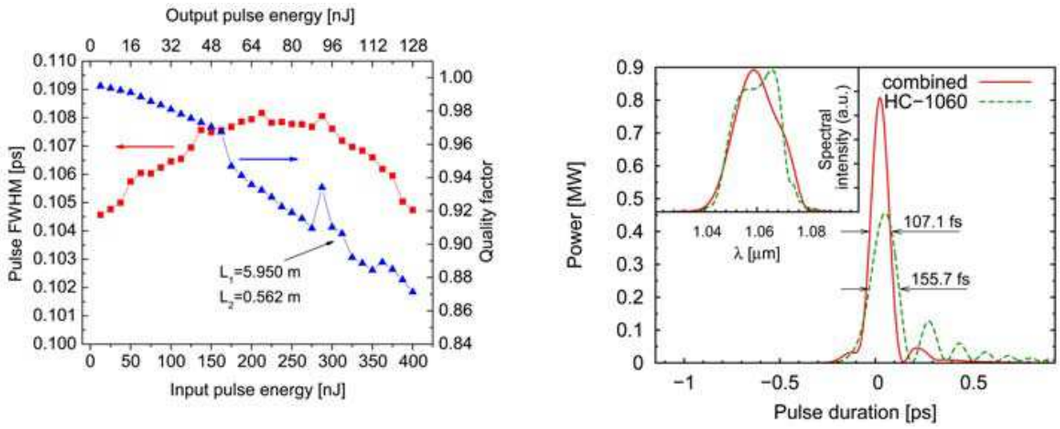

(a) (b)

Fig. 17. (a) Pulse full width at half maximum (FWHM) evaluation as a function of pulse energy with $GDD_0 = 5 \cdot 10^5$ fs² input chirp; black arrow shows the regular (L_1) and RDS fiber lengths (L_2) at 90% quality factor, (b) pulse shapes with combined and HC-1060 type fibre compressors.

7. Conclusion

We have given a qualitative explanation of adopting one-dimensional Gires-Tournois interferometers (GTI) in two-dimensional photonic bandgap (PBG) structures. We showed that by properly adjusting one or two resonant layers around the fibre core in solid- or hollow core bandgap fibers may result a tailored dispersion profile even reversed dispersion slope (RDS).
Finite element analyses confirmed that the dispersion profile of PBG fibres can be tailored effectively by the application of resonant layers for the propagating fundamental mode. And this works for higher order modes as well. We calculated the dispersion properties of solidcore Bragg and all-silica photonic crystal fibers as well as hollow-core Bragg and photonic crystal fibres with honey-comb cladding structure. Negative dispersion slope compared to the canonical form of bandgap guidance as well as flat and nearly zero dispersion profiles are obtained with relatively low losses. Fiber properties were also analyzed. After structural optimization, low coupling losses between two fibres, with and without GTI, also demonstrated. The obtained dispersion profiles showing negative dispersion slope over 100 nm wavelength regions may yield new perspectives in dispersion management even if the increased nonlinearity and propagation loss of hollow-core RDS fibres somewhat decrease the transmittable intensities. Further optimization and investigation of the presented structures may improve their physical properties. The propagation and compression of pre-chirped, broadband Gaussian pulses confirmed the validity of further developments on RDS PBG fibres.

8. References

Agrawal, G. P. (2007). *Nonlinear Fiber Optics, fourth edition*, Academic, San Diego, CA.
Birks, T. A., Knight, J. C. & Russell, P. S. J. (1997). Endlessly single-mode photonic crystal fiber, *Opt. Lett.* 22: 961–963.

Bouwmans, G., Luan, F., Knight, J., Russell, P. S. J., Farr, L., Mangan, B. & Sabert, H. (2003). Properties of a hollow-core photonic bandgap fiber at 850 nm wavelength, *Opt. Express* 11: 1613–1620.

Cregan, R. F., Mangan, B. J., Knight, J. C., Birks, T. A., Russell, P. S. J., Roberts, P. J. & Allan, D. C. (1999). Single-mode photonic band gap guidance of light in air, *Science* 285: 1537–1539.

de Matos, C., Taylor, J., Hansen, T., Hansen, K. & Broeng, J. (2003). All-fiber chirped pulse amplification using highly-dispersive air-core photonic bandgap fiber, *Opt. Express* 11: 2832–2837.

Dianov, E. M., Likhachev, M. E. & Février, S. (2009). Solid-core photonic bandgap fibers for high-power fiber lasers, *IEEE J. Sel. Topics Quantum Electron.* 15: 20–29.

Egorova, O. N., Semjonov, S. L., Kosolapov, A. F., Denisov, A. N., Pryamikov, A. D., Gaponov, D. A., Biriukov, A. S., Dianov, E. M., Salganskii, M. Y., Khopin, V. F., Yashkov, M. V., Gurianov, A. N. & Kuksenkov, D. V. (2008). Single-mode all-silica photonic bandgap fiber with 20 μm mode-field diameter, *Opt. Express* 16: 11735–11740.

Engeness, T., Ibanescu, M., Johnson, S., Weisberg, O., Skorobogatiy, M., Jacobs, S. & Fink, Y. (2003). Dispersion tailoring and compensation by modal interactions in OmniGuide fibers, *Opt. Express* 11: 1175–1196.

Fang, Q., Wang, Z., Jin, L., Liu, J., Yue, Y., Liu, Y., Kai, G., Yuan, S. & Dong, X. (2007). Dispersion design of all-solid photonic bandgap fiber, *J. Opt. Soc. Am. B* 24: 2899–2905.

Fekete, J., Várallyay, Z. & Szipőcs, R. (2008). Design of high-bandwidth one- and two-dimensional photonic bandgap dielectric structures at grazing incidence of light, *Appl. Opt.* 47: 5330–5336.

Ferrando, A., Silvestre, E.,Miret, J. J. & Andrés, P. (2000). Nearly zero ultraflattened dispersion in photonic crystal fibers, *Opt. Lett.* 25: 790–792.

Foroni, M., Passaro, D., Poli, F., Cucinotta, A., Selleri, S., Lægsgaard, J. & Bjarklev, A. (2007). Confinement loss spectral behavior in hollow-core Bragg fibers, *Opt. Lett.* 32: 3164–3166.

Foster, M. A., Gaeta, A. L., Cao, Q. & Trebino, R. (2005). Soliton-effect compression of super-continuum to few cycle durations in photonic nanowires, *Opt. Express* 13: 6848–6855.

Hensley, C. J., Ouzounov, D. G., Gaeta, A. L., Venkataraman, N., Gallagher,M. T. & Koch, K.W. (2007). Silica-glass contribution to the effective nonlinearity of hollow-core photonic band-gap fibers, *Opt. Express* 15: 3507–3512.

Humbert, G., Knight, J. C., Bouwmans, G., Russell, P. S. J., Williams, D. P., Roberts, P. J. & Mangan, B. J. (2004). Hollow core photonic crystal fiber for beam delivery, *Opt. Express* 12: 1477–1484.

Jasapara, J., Bise, R., Her, T. & Nicholson, J. W. (2003). Effect of mode cut-off on dispersion in photonic bandgap fibers, *Optical Fiber Communication Conference, Technical Digest*, Optical Society of America, p. ThI3.

Jasapara, J., Her, T. H., Bise, R., Windeler, R. & DiGiovanni, D. J. (2003). Group-velocity dispersion measurements in a photonic bandgap fiber, *J. Opt. Soc. Am. B* 20: 1611–1615.

John, S. (1987). Strong localization of photons in certain disordered dielectric superlattices, *Phys. Rev. Lett.* 58: 2486–2489.

Knight, J. C., Birks, T. A., Cregan, R. F., Russell, P. S. J. & de Sandro, J. P. (1998). Large mode area photonic crystal fibre, *Electron. Lett.* 34: 1347–1348.

Knight, J. C., Birks, T. A., Russell, P. S. J. & Atkin, D. M. (1996). All-silica single-mode optical fiber with photonic crystal cladding, *Opt. Lett.* 21: 1547–1549.

Knight, J. C., Broeng, J., Birks, T. A. & Russell, P. S. J. (1998). Photonic band gap guidance in optical fibres, *Science* 282: 1476–1478.

Kuhl, J. & Heppner, J. (1986). Compression of femtosecond optical pulses with dielectric multilayer interferometers, *IEEE Trans. Quant. Electron.* QE-22: 182–185.

Lægsgaard, J., Mortensen, N. A., Riishede, J. & Bjarklev, A. (2003). Material effects in air-guiding photonic bandgap fibers, *J. Opt. Soc. Am. B* 20: 2046–2051.

Lægsgaard, J. & Roberts, P. J. (2008). Dispersive pulse compression in hollow-core photonic bandgap fibers, *Opt. Express* 16: 9628–9644.

Lægsgaard, J., Roberts, P. J. & Bache,M. (2007). Tailoring the dispersion properties of photonic crystal fibers, *Optical and Quantum Electronics* 39: 995–1008.

Lim, H., Ilday, F. & Wise, F. (2002). Femtosecond ytterbium fiber laser with photonic crystal fiber for dispersion control, *Opt. Express* 10: 1497–1502.

Limpert, J., Liem, A., Reich, M., Schreiber, T., Nolte, S., Zellmer, H., Tünnermann, A., Broeng, J., Petersson, A. & Jakobsen, C. (2004). Low-nonlinearity single-transverse-mode ytterbium-doped photonic crystal fiber amplifier, *Opt. Express* 12: 1313–1319.

Limpert, J., Schmidt, O., Rothhardt, J., Röser, F., Schreiber, T., Tünnermann, A., Ermeneux, S., Yvernault, P. & Salin, F. (2006). Extended single-mode photonic crystal fiber lasers, *Opt. Express* 14: 2715–2720.

Macleod, H. A. (2001). *Thin-film optical filters third edition*, J WArrowsmith Ltd., Bristol. Mogilevtsev, D., Birks, T. A. & Russell, P. S. J. (1998). Group-velocity dispersion in photonic crystal fiber, *Opt. Lett.* 23: 1662–1664.

Mortensen, N. A., Nielsen, M. D., Folkenberg, J. R., Petersson, A. & Simonsen, H. R. (2003). Improved large-mode-area endlessly single-mode photonic crystal fibers, *Opt. Lett.* 28: 393–395.

Müller, D.,West, J. & Koch, K. (2002). Interferometric chromatic dispersion measurement of a photonic band-gap fiber, *in* A. K. Dutta, A. A. S. Awwal, N. K. Dutta & K. Okamoto (eds), *Active and Passive Components for WDM communications II*, Vol. 4870, SPIE, pp. 395–403.

Murao, T., Saitoh, K. & Koshiba, M. (2008). Structural optimization of air-guiding photonic bandgap fibers for realizing ultimate low loss waveguides, *J. Lightwave Technol.* 26: 1602–1612.

Nielsen, C. K., Jespersen, K. G. & Keiding, S. R. (2006). "a 158 fs 53 nJ fiber-laser system at 1μm using photonic bandgap fibers for dispersion control and pulse compression, *Opt. Express* 14: 6063–6068.

Ouzonov, D. G., Ahmad, F. R., Müller, D., Venkataraman, N., Gallagher, M. T., Thomas, M. G., Silcox, J., Koch, K. W. & Gaeta, A. L. (2003). Generation of megawatt optical solitons in hollow-core photonic band-gap fibers, *Science* 301: 1702–1704.

Ouzounov, D., Hensley, C., Gaeta, A., Venkateraman, N., Gallagher, M. & Koch, K. (2005). Soliton pulse compression in photonic band-gap fibers, *Opt. Express* 13: 6153–6159.

Ranka, J. K., Windeler, R. S. & Stentz, A. J. (2000). Visible continuum generation in air-silica microstructure optical fibers with anomalous dispersion at 800 nm, *Opt. Lett.* 25: 25– 27.

Roberts, P. J. (2007). Control of dispersion in hollow core photonic crystal fibers, *Conference on Lasers and Electro-Optics (CLEO 2007)*, CLEO, p. CWF2.

Roberts, P. J., Couny, F., Sabert, H., Mangan, B. J., Williams, D. P., Farr, L., Mason, M. W., Tomlinson, A., Birks, T. A., Knight, J. C. & Russell, P. S. J. (2005). Ultimate low loss of hollow-core photonic crystal fibres, *Opt. Express* 13: 236–244.

Roberts, P. J., Williams, D. P., Mangan, B. J., Sabert, H., Couny, F., Wadsworth, W. J., Birks, T. A., Knight, J. C. & Russell, P. S. J. (2005). Realizing low loss air core photonic crystal fibers by exploiting an antiresonant core surround, *Opt. Express* 13: 8277–8285.

Ruehl, A., Prochnow, O., Engelbrecht, M., Wandt, D. & Kracht, D. (2007). Similariton fiber laser with a hollow-core photonic bandgap fiber for dispersion control, *Opt. Lett.* 32: 1084–1086.

Saitoh, K., Florous, N. J., Murao, T. & Koshiba, M. (2007). Realistic design of large-hollow-core photonic band-gap fibers with suppressed higher order modes and surface modes, *J. Lightwave Technol.* 25: 2440–2447.

Saitoh, K. & Koshiba, M. (2003). Leakage loss and group velocity dispersion in air-core photonic bandgap fibers, *Opt. Express* 11: 3100–3109.

Saitoh, K., Koshiba, M., Hasegawa, T. & Sasaoka, E. (2003). Chromatic dispersion control in photonic crystal fibers: application to ultra-flattened dispersion, *Opt. Express* 11: 843– 852.

Saitoh, K., Mortensen, N. A. & Koshiba, M. (2004). Air-core photonic band-gap fibers: the impact of surface modes, *Opt. Express* 12: 394–400.

Shephard, J., MacPherson, W., Maier, R., Jones, J., Hand, D., Mohebbi, M., George, A., Roberts, P. & Knight, J. (2005). Single-mode mid-ir guidance in a hollow-core photonic crystal fiber, *Opt. Express* 13: 7139–7144.

Stephens, T. J., Maier, R. R., Barton, J. S. & Jones, J. D. C. (2004). Fused silica hollow-core photonic crystal fibre for mid-infrared transmission, *Conference on Lasers and Electro-Optics (CLEO 2004)*, CLEO, p. CPDD4.

Szipőcs, R., Kőházi Kis, A., Lakó, S., Apai, P., Kovács, A. P., DeBell, G., Mott, L., Louderback, A. W., Tikhonravov, A. V. & Trubetskov, M. K. (2000). Negative dispersion mirrors for dispersion control in femtosecond lasers: chirped dielectric mirrors and multi-cavity Gires-tournois interferometers, *Appl. Phys. B* 70: S51–S57.

Tong, L.M., Gattass, R. R., Ashcom, J. B., He, S. L., Lou, J. Y., Shen, M. Y., Maxwell, I. & Mazur, E. (2003). Subwavelength-diameter silica wires for low-loss optical wave guiding, *Nature* 426: 816–819.

Várallyay, Z., Fekete, J., Bányász, Á. & Szipőcs, R. (2007). Optimizing input and output chirps up to the third-order for sub-nanojoule, ultra-short pulse compression in small core area PCF, *Appl. Phys. B* 86(4): 567–572.

Várallyay, Z., Fekete, J. & Szipőcs, R. (2008a). Higher-order mode photonic bandgap fibers for dispersion control, *CLEO Conference, San Jose, CA*, OSA, p. JThA48.

Várallyay, Z., Fekete, J. & Szipőcs, R. (2008b). Higher-order mode photonic bandgap fibers with reversed dispersion slope, *OFC/NFOEC Conference 2008, San Diego, CA*, OSA, p. JWA8.

Várallyay, Z., Saitoh, K., Fekete, J., Kakihara, K., Koshiba, M. & Szipőcs, R. (2008). Reversed dispersion slope photonic bandgap fibers for broadband dispersion control in femtosecond fiber lasers, *Opt. Express* 16: 15603–15616.

Várallyay, Z., Saitoh, K., Szabó, Á. & Szipőcs, R. (2009). Photonic bandgap fiberswith resonant structures for tailoring the dispersion, *Opt. Express* 17: 11869–11883.

Vienne, G., Xu, Y., Jakobsen, C., Deyerl, H. J., Jensen, J., Sorensen, T., Hansen, T., Huang, Y., Terrel, M., Lee, R., Mortensen, N., Broeng, J., Simonsen, H., Bjarklev, A. & Yariv, A. (2004). Ultra-large bandwidth hollow-core guiding in all-silica Bragg fibers with nano-supports, *Opt. Express* 12: 3500–3508.

Vincetti, L., Maini, M., Poli, F., Cucinotta, A. & Selleri, S. (2006). Numerical analysis of hollow core photonic band gap fibers with modified honeycomb lattice, *Opt. and Quantum Electron.* 38: 903–912.

Yablonovitch, E. (1987). Inhibited spontaneous emission in solid-state physics and electronics, *Phys. Rev. Lett.* 58: 2059–2062.

Yeh, P., Yariv, A. & Marom, E. (1978). Theory of Bragg fiber, *J. Opt. Soc. Am.* 68: 1196–1201.

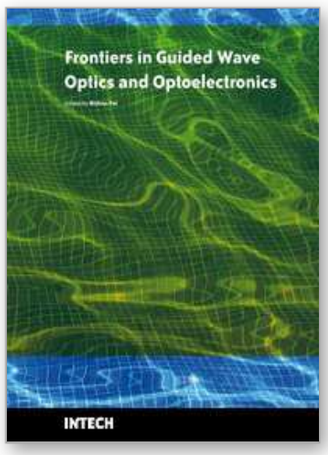

Frontiers in Guided Wave Optics and Optoelectronics

Edited by Bishnu Pal

ISBN 978-953-7619-82-4
Hard cover, 674 pages
Publisher InTech
Published online 01, February, 2010
Published in print edition February, 2010

As the editor, I feel extremely happy to present to the readers such a rich collection of chapters authored/co-authored by a large number of experts from around the world covering the broad field of guided wave optics and optoelectronics. Most of the chapters are state-of-the-art on respective topics or areas that are emerging. Several authors narrated technological challenges in a lucid manner, which was possible because of individual expertise of the authors in their own subject specialties. I have no doubt that this book will be useful to graduate students, teachers, researchers, and practicing engineers and technologists and that they would love to have it on their book shelves for ready reference at any time.

INTECH
open science | open minds

InTech Europe
University Campus STeP Ri
Slavka Krautzeka 83/A
51000 Rijeka, Croatia
Phone: +385 (51) 770 447
Fax: +385 (51) 686 166
www.intechopen.com

InTech China
Unit 405, Office Block, Hotel Equatorial Shanghai
No.65, Yan An Road (West), Shanghai, 200040, China
中国上海市延安西路65号上海国际贵都大饭店办公楼405单元
Phone: +86-21-62489820
Fax: +86-21-62489821

IntechOpen